

**ISTANBUL TECHNICAL UNIVERSITY ★ GRADUATE SCHOOL OF SCIENCE**  
**ENGINEERING AND TECHNOLOGY**

**TOWARDS FULLY 3D-PRINTED MINIATURIZED CONFOCAL IMAGER**



**M.Sc. THESIS**

**Janset SAVAŞ**

**Department of Electronics and Communication Engineering**

**Electronic Engineering Programme**

**JUNE 2017**



**ISTANBUL TECHNICAL UNIVERSITY ★ GRADUATE SCHOOL OF SCIENCE**  
**ENGINEERING AND TECHNOLOGY**

**TOWARDS FULLY 3D-PRINTED MINIATURIZED CONFOCAL IMAGER**



**M.Sc. THESIS**

**Janset SAVAŞ**  
**504151209**

**Department of Electronics and Communication Engineering**

**Electronic Engineering Programme**

**Thesis Advisor: Assistant Prof. Onur FERHANOĞLU**  
**Thesis Co-Advisor: Assistant Prof. Yiğit Dağhan GÖKDEL**

**JUNE 2017**



**İSTANBUL TEKNİK ÜNİVERSİTESİ ★ FEN BİLİMLERİ ENSTİTÜSÜ**

**3 BOYUTLU YAZICI İLE ÜRETİLMİŞ MİNYATÜRİZE KONFOKAL  
GÖRÜNTÜLEYİCİ**

**YÜKSEK LİSANS TEZİ**

**Janset SAVAŞ  
504151209**

**Elektronik ve Haberleşme Mühendisliği Anabilim Dalı**

**Elektronik Mühendisliği Programı**

**Tez Danışmanı: Yrd. Doç. Dr. Onur FERHANOĞLU  
Eş Danışman: Yrd. Doç. Dr. Yiğit Dağhan GÖKDEL**

**HAZİRAN 2017**



Janset Savaş, a M.Sc. student of İTÜ Graduate School of Science Engineering and Technology student ID 504151209, successfully defended the thesis entitled “TOWARDS FULLY 3D-PRINTED MINIATURIZED CONFOCAL IMAGER”, which she prepared after fulfilling the requirements specified in the associated legislations, before the jury whose signatures are below.

**Thesis Advisor :**      **Assistant Prof. Onur FERHANOĞLU** .....  
Istanbul Technical University

**Co-advisor :**            **Assistant Prof. Yiğit Dağhan GÖKDEL** .....  
Istanbul Bilgi University

**Jury Members :**        **Associate Prof. Mesut Kartal** .....  
Istanbul Technical University

**Assistant Prof. Mustafa Berke Yelten** .....  
Istanbul Technical University

**Assistant Prof. Baykal Sarıoğlu** .....  
Istanbul Bilgi University

**Date of Submission : 5 May 2017**

**Date of Defense : 7 June 2017**







*To my family,*



## **FOREWORD**

In this thesis, a prototype of a low cost medical imaging device that is a 3D printed confocal endoscope has been developed.

For all their efforts and support, I'd like to thank my advisor Onur Ferhanođlu, my co-advisor and undergrad Assistant Prof. Yiđit Dađhan Gökdel, and Assistant Prof. Fehmi Çivitçi. Lastly, I would like to thank my jury members addition to my advisors, Associate Prof. Mesut Kartal, Assistant Prof. Mustafa Berke Yelten, and Assistant Prof. Baykal Sarıođlu.

I would like to thank Ahmet Turan Talas from Bođaziçi University for his support in manufacturing all 3D-printed parts. Y. Dađhan Gökdel acknowledges support by TUBITAK under grant 113S114. Onur Ferhanođlu acknowledges support by TUBITAK under grant 215E259 and Istanbul Technical University Research Fund (ITU BAP # 39124).

June 2017

Janset SAVAŞ  
Electronic Engineer



## TABLE OF CONTENTS

	<u>Page</u>
<b>FOREWORD</b> .....	ix
<b>TABLE OF CONTENTS</b> .....	xi
<b>ABBREVIATIONS</b> .....	xiii
<b>SYMBOLS</b> .....	xv
<b>LIST OF TABLES</b> .....	xvii
<b>LIST OF FIGURES</b> .....	xix
<b>SUMMARY</b> .....	xxi
<b>ÖZET</b> .....	xxiii
<b>1. INTRODUCTION</b> .....	1
<b>2. FABRICATION OF 3D-PRINTED LENS</b> .....	3
2.1 Fabrication of 3d-Printed Bulky Lens.....	3
2.2 Fabrication of Miniaturized Imager Lens.....	8
<b>3. 3D PRINTED MICROSCANNER</b> .....	11
<b>4. 3D-PRINTED HOUSING, SYSTEM INTEGRATION AND     CHARACTERIZATION</b> .....	17
<b>5. CONCLUSION AND DISCUSSION</b> .....	25
<b>REFERENCES</b> .....	29
<b>APPENDICES</b> .....	33
APPENDIX A .....	34
<b>CURRICULUM VITAE</b> .....	39



## ABBREVIATIONS

<b>MEMS</b>	: Micro Electro Mechanical Systems
<b>FOV</b>	: Field Of View
<b>FHWM</b>	: Full Width Half Maximum
<b>NA</b>	: Numerical Aperture
<b>GRIN</b>	: Gradient Index
<b>OCT</b>	: Optical Coherence Tomography
<b>CCD</b>	: Charge Coupled Device
<b>CMOS</b>	: Complementary Metal Oxide Semiconductor
<b>HD</b>	: High Definition
<b>LDV</b>	: Laser Doppler Vibrometer





## SYMBOLS

$\delta xy$  : Spot Size  
 $\lambda$  : Wavelength  
 $f$  : Focal Length





**LIST OF TABLES**

	<u>Page</u>
<b>Table 3.1</b> : Detailed Dimensions Of The Microscanner. ....	<b>14</b>
<b>Table 5.1</b> : Comparison with Similar Studies .....	<b>28</b>





## LIST OF FIGURES

	<u>Page</u>
<b>Figure 2.1</b> : 3D Printed Lens.....	6
<b>Figure 2.2</b> : Processed 3D Printed Lens.....	6
<b>Figure 2.3</b> : Commercial Glass Lens.....	7
<b>Figure 2.4</b> : Comparison of Lens Surfaces.....	7
<b>Figure 2.5</b> : Lens Focus With Support (Top), Illustrating Central Cross Sections Of Top Image (Bottom).....	8
<b>Figure 2.6</b> : Periodic Pattern Of Support Structure.....	9
<b>Figure 2.7</b> : Lens Focus Without Support (Top), Illustrating Central Cross Sections Of Top Image (Bottom).....	10
<b>Figure 2.8</b> : i. Commercial 3D Printed Lens, ii.3D Printed Lens (This Work), iii.Commercial Glass Lens.....	11
<b>Figure 2.9</b> : Spot Comparison Graph of Commercial 3D Printed Lens, 3D Printed Lens (This Work), Commercial Glass Lens.....	12
<b>Figure 3.1</b> : CAD Drawing Of The Designed Microscanner Structure ...	13
<b>Figure 3.2</b> : The Manufactured Microscanner Structure.....	14
<b>Figure 3.3</b> : The Frequency Response Of The 3D Printed Scanner, As Acquired By The LDV Unit. FEM Modal Analysis Results Are Also Included Above Each Corresponding Mode .....	15
<b>Figure 3.4</b> : Von Mises Stress Analysis Of The Rectangular Flexure.....	16
<b>Figure 3.5</b> : Von Mises Stress Analysis Of The Elliptic And Tapered Flexure Revealing $> x2$ Times Reduced Stress Levels. ....	16
<b>Figure 4.1</b> : The Housing Unit in Which The Components Are Assembled CAD Drawing. The Shown Components Are: 1) Scanner, 2) Coil, 3) Lens, 4) Electrical Interconnect Channel, 5) Input Fiber.....	19
<b>Figure 4.2</b> : The Housing Unit in Which The Components Are Assembled Photo Of The Manufactured Unit. The Shown Components Are: 1) Scanner, 2) Coil, 3) Lens, 4) Electrical Interconnect Channel, 5) Input Fiber.....	20
<b>Figure 4.3</b> : Characterization Setup (M1, M2 : Mirrors, BS : Beam Splitter, PD : Photodetector, OBJ : Objective Lens) Used in Acquiring Line Scans From The Target.....	22
<b>Figure 4.4</b> : Lissajous Scan Pattern of 3D Printed & Miniaturized Confocal Imager .....	23
<b>Figure 4.5</b> : USAF 1951 Resolution Target (4th Group 1st Element Marked in Box).....	23
<b>Figure 4.6</b> : The Distance-Intensity Graph Acquired From the 4th Group 1st Element .....	24
<b>Figure 4.7</b> : Close-Up View of the First Step Showing in Fig 4.7, And Its Spatial Derivative That Reveals A FWHM Resolution Of 11.4- $\mu\text{m}$ . ...	25
<b>Figure A.1</b> : 3D Printing Steps.....	33
<b>Figure A.2</b> : AutoCAD Interface... ..	34
<b>Figure A.3</b> : Objet260 Connex 3D Printer....	34
<b>Figure A.4</b> : Objet Studio's Interface and the Tray .....	39
<b>Figure A.5</b> : Setting Position.....	35
<b>Figure A.6</b> : Selection of Materials.....	36
<b>Figure A.7</b> : Starting the Printing Process .....	36



## **TOWARDS FULLY 3D-PRINTED MINIATURIZED CONFOCAL IMAGER**

### **SUMMARY**

In this project a low cost, miniaturized confocal imager, consisting of 3D printed functional optical and electromechanical parts, namely, a laser scanner, a lens, and the housing is presented. The imager parts are printed from polymer material which is extremely affordable. This allows the device to be designed as disposable.

The electromechanical scanning unit within the endoscopic device, having 10x10 mm<sup>2</sup> frame size, is electromagnetically actuated in two dimensions, via a magnet that is attached to the 3D printed scanner using epoxy glue and an external miniaturized coil to work with it.

3D Printing offers extensive fabrication capabilities such as less than 20 micron resolution, processing, multi-dimensional tapering and printing hollow structures with precision. These capabilities allowed us to tailor the first two vibration modes as out-of-plane displacement and torsion movement, while pushing other undesired mechanical modes to higher frequencies.

The scanner employs lissajous scan, with 180 Hz and 315 Hz scan frequencies in the orthogonal directions where we achieved  $\pm 8^\circ$  and  $\pm 4^\circ$  optical scan angles, respectively, with less than 100 mA drive current. The lens, which has a 6 mm diameter and 10 mm focal length, is 3D printed with veroclear material, then polished to obtain an optical quality surface. Polishing process was achieved in two steps which are sanding and applying an emery polisher with pressure.

Surface profiler measurements, together with imaging experiments reveal only two times increase in rms roughness and a comparable focused spot diameter (less than 10% difference), as opposed to a commercial glass lens having identical structure and almost identical focal length. Scanner and lens units, together with the external coil were press-fitted into a 3D-printed housing having 17 mm width, which is comparable to many of the miniaturized MEMS based laser scanning imagers. With further development, the 3D printed confocal imager can serve as a disposable diagnostic tool for the clinic.





## ÜÇ BOYUTLU YAZICI İLE ÜRETİLMİŞ MİNYATÜRİZE KONFOKAL GÖRÜNTÜLEYİCİ

### ÖZET

Biyolojik örneklerin mikroskopik görüntülenmesi, konfokal mikroskop, multi-foton mikroskop ve optik koherans tomografisi gibi lazer taramalı mikroskop teknikleri tarafından sürdürülmektedir. Mikro-elektromekanik sistemlerdeki gelişmeler ve yüksek kalite optic ve opto-mekanik elemanların üretilmeye başlaması ile bu cihazların minyatürize edilerek portatif hatta endoskopik görüntüleyicilere dönüşmesine imkan sağlamıştır.

Bu görüntüleyiciler sadece güvenilir hücresel görüntüler sağlamakla kalmayıp ağız boşluğu, rahim, soluk borusu, sindirim sistemi boşlukları gibi ulaşılması zor dokuları görüntülemeye küçük boyutları sayesinde imkan sağlamıştır.

Minyatürize mikroskopik cihazlarda fiber optik kablolar, mikro-elektromekanik sistem tarayıcı aynalar, piezo ile hareketlendirilen tarayıcılar gibi bir çok yeni teknoloji kullanılmaktadır. Fiber kablolar doku görüntüleme için haritalandırma yöntemini kullanır. Fiberin bir ucu dokuya temas ederken diğer ucu bir CCD ya da CMOS algılayıcıya görüntü bilgisini ulaştırır. Bu teknolojiye tarama olmadığından minyatürize etme en yüksek seviyededir.

Mikro-elektromekanik sistemler ise ışık huzmelerini belli frekanslarda yansıtarak tarama işlemi yapmaktadır. Yüksek mekanik tarama frekansları ve tarama açıları sayesinde çok yüksek çözünürlükte görüntüler mikro-elektromekanik tarayıcılar kullanılan görüntüleyicilerde elde edilebilmektedir.

Piezo tarama tabanlı fiber proplar lazer taramalı görüntüleyicilerde sık kullanılmaktadır. Sıkıştırılmış geometrisi ve küçük boyutları kullanım alanlarını arttırmaktadır. Piezo tüp malzeme özelliğinden dolayı kendine uygulanan voltajı mekanik harekete çevirir. Bu malzemeye kendi mekanik rezonans frekansında sinyal verildiğinde fiberden gelen ışık spiral bir tarama deseni oluşturmaktadır.

Mikro-elektromekanik sistem, piezo silindir tarayıcı, fiber tarayıcı gibi tüm bu minyatürize tarayıcı teknolojilerinde tarama için gerekli donanımlar, mikro-optik elemanlar, lensler göz önüne alındığında bütçe çok yüksek rakamlara çıkmaktadır. Bu bütçe görüntüleyici sistemlerin hem yaygın olmamasına hem de tek kullanımlık (kullan-at) sistemler halinde tasarlanmasına imkan vermemektedir.

Bu çalışmada düşün bütçeli minyatürize bir konfokal görüntüleyici sunulmaktadır. Görüntüleyici 3 boyutlu yazıcı ile üretilmiş fonksiyonel optik ve elektromekanik parçalardan oluşmaktadır. 3 boyutlu yazıcılar bilgisayarda tasarlanmış modelleri katman katman polimer yayma yöntemi ile basmaktadır. Basılacak model tamamen kullanıcının tasarımına bağlıdır. Bu çalışmada tanıtılan cihaz lazer tarayıcısı, lens ve dış gövde olmak üzere üç adımda üretilmiştir. Görüntüleyicinin parçaları polimer ile üretildiğinden cihaz oldukça düşük maliyetlidir. Bu özelliğiyle cihaz tek kullanımlık olarak tasarlanabilmektedir.

Endoskopik görüntüleyicinin içerisindeki elektromekanik tarayıcı ünitesi  $10 \times 10 \text{ mm}^2$  çerçeve boyuna sahiptir ve tarayıcıya sabitlenmiş bir mıknatıs ve mini bir bobin kullanılarak elektromanyetik olarak iki boyutta uyarılmaktadır. Bu uyarım sonucu iki boyutlu yüksek kalitede görüntüler alınması mümkün kılınmıştır. Boyutu ve performansı ile üretilen tarayıcı, ticari olarak ulaşılabilen yüksek bütçeli tarayıcılarla karşılaştırılabilir tarama özelliklerine sahiptir.

Üç boyutlu yazıcı teknolojisi 20 mikron altı kapsamlı üretim olanakları sunmaktadır. Birçok temiz oda teknolojisinden farklı olarak 3 boyutlu yazıcı sadece düzlemsel değil, çok boyutlu, konik, içi boş (oyuk) üretimlere de olanak sağlamaktadır. Bu olanakları kullanarak ilk iki titreşim modu düzlem dışı titreşim ve burulma (kıvrılma) olarak tasarlanmıştır. İstenmeyen titreşim modları daha yüksek frekanslara ötelenmiştir.

Tarayıcı 180 Hz ve 315 Hz frekanslarında dikey eksenlerde lissajous tipi tarama yapmaktadır. Bu frekanslar 3 boyutlu yazıcının sağladığı üretim imkanları sayesinde elde edilebilmiştir. 180 Hz'de düzlem dışı tarama denen tarama tipi ile dikey tarama sağlanmaktadır. 315 Hz'de ise kıvrılma (bükülme) tipi tarama ile yatay tarama sağlanmıştır.

Lissajous tarama iki sinüs sinyalinin birleşimi ile bu iki boyutta elde edilmektedir. 100 mA ve daha az akımlarda optik tarama açıları sırasıyla  $\pm 8^\circ$  and  $\pm 4^\circ$  olarak hesaplanmıştır.

Tarayıcının karakteristik özellikleri lazer doppler vibrometrede (LDV) test edilmiştir. LDV cihazı içindeki lazeri tarayıcının aynasına doğrultmakta ve yansıma ile gönderilen ışının faz farklarına dayanarak tarayıcının titreşiminin güvenilir biçimde modellemektedir. Bu testler sonucunda tarayıcının frekans cevabının simülasyonlarla ve cihazın tasarımı ile uyumlu olduğu tespit edilmiştir.

Lens üretiminde veroclear adlı şeffaf malzeme kullanılmıştır. Üretilen polimer lens 6 mm çapında ve 10 mm odak uzunluğuna sahiptir. Çıktı alındıktan sonra lens optik kalitede bir yüzey elde etmek için bir dizi işlemden geçmiştir. Bu işlemler sırasıyla ince zımpara ve kimyasal yüzey cilası uygulanması şeklindedir.

Zımparalama işlemi 2000 kumluk zımpara ile saf su içerisinde yapılmıştır. Lensin iki yüzeyi de 15'er dakika boyunca zımparalanmıştır. Bundan sonra kurulan lense Meguiars 101 tipi çizik giderici cila pamuk yardımı ile yüksek basınçla uygulanmıştır.

Bu işlemlerden sonra lensin yüzeyi profilometre ile ölçülmüş, bunun yanı sıra görüntüleme deneyleri yapılmıştır. Bu deney ve ölçümler göstermiştir ki lens aynı boyut ve odak uzunluğuna sahip ticari cam lens ile karşılaştırıldığında sadece iki kat rms pürüzü ve %10 hata payı içerisinde bir odak benek çapına sahiptir.

Tarayıcı ve lens üniteleri mini bobin ile beraber 3 boyutlu yazıcı ile üretilmiş 17 mm genişlik 33m uzunluk ve 12 mm derinliğe sahip dış gövdeye preslenerek oturtulmuştur. Tüm cihaz oluşturulduktan sonra USAF 1951 çözünürlük hedefi üzerinde görüntüleme deneyleri yapılmıştır.

Bu deneyler sonucu cihazın 4.grup 1.elemente kadar çözebildiği gözlenmiştir. Bu element 30 mikrometre boyunda üç dikey çizgiden oluşmaktadır. Bu okumanın türevi üzerinde yapılan incelemeler cihazın çözünürlüğünü 11.4 mikrometre olarak göstermektedir.

Bu sonuçlar mikro-elektromekanik teknolojisi kullanılan ve ticari olarak ulaşılabilir cihazlarla karşılaştırılabilir seviyededir. Daha ileri çalışma ile 3 boyutlu yazıcı ile üretilmiş bu konfokal görüntüleyici, bir kullan at endoskop olarak klinik ortamda tanı cihazı olarak kullanılabilir.

3 boyutlu yazıcı teknolojisinde yaşanan gelişmeler gelecekte cihazın tamamen 3 boyutlu yazıcı ile üretilmesine imkan sağlayacaktır. Geçtiğimiz yıllarda keşfedilen magnetik polimer ve gümüş mürekkep ile doldurma yöntemleri bu çalışmada tanıtılan sistemde kullanılan bobin ve mıknatısa bağımlılığı ortadan kaldıracaktır.



## 1. INTRODUCTION

Microscopic imaging of biological specimens has been performed through laser scanning microscopy techniques such as confocal microscopy [1], Optical Coherence Tomography (OCT) [2], and multi-photon microscopy [3]. The advances in Micro-electro-mechanical-systems (MEMS) and fiber-optic technology, together with the development of high-quality micro-optical components have allowed for miniaturization of these microscopy techniques into handheld probes and endoscopes [4].

Such miniaturized imaging tools not only offer a robust, cellular scale imaging platform for the healthcare personnel, but also enable accessing tissue sites in the oral cavity, cervix and the GI tract that are otherwise difficult to access, owing to their compact size. Miniaturized microscopic tools have benefited the use of fiber optic bundles, MEMS micro-scanners, rotary actuators, and piezo-actuated fiber scanners. Fiber-bundles have been employed for tissue imaging, with their frontal end contacting the tissue and with the distal end mapped on a CCD or CMOS sensor array [5]. The absence of scanning parts enables utmost miniaturization of fiber-bundle imagers.

Other miniaturized imaging tools have utilized MEMS to scan the light beam in a forward- or side-viewing fashion. Thanks to their high mechanical scan frequency and scan angles, MEMS devices offer unprecedented number of resolvable spots potentially providing HD quality images [6,7].

Furthermore, rotary actuators have been particularly useful in imaging large epithelial areas within the esophagus, with the help of a balloon mechanism to center the probe within the hollow cavity [8,9]. Thanks to their compact geometry and simple in-line architecture, piezo-scanning based fiber probes have been exploited in laser scanning endoscopy applications [10,11]. The piezo-tube, which converts applied voltage to mechanical movement, is driven at the mechanical resonance of the extended fiber to create a spiral scan pattern. Yet, in all of the aforementioned miniaturized light scanning tools, the cost of the scanning (MEMS, rotary actuators, piezo-cylinder

scanner) or fiber bundle units, together with other micro-optical elements (miniaturized lenses), significantly contribute to the overall budget of the developed imaging tool, hampering the widely and disposable use of these devices.

Three Dimensional (3D) printing has advanced as a versatile technique to sequentially fabricate various materials layer-by-layer in accordance with a computer-aided-design (CAD) model. Although the technique is widely used in manufacturing static frames to encapsulate and relatively align other functional components (such as housing of a laser scanning probe) recent advances have facilitated the production of mechanically movable elements for sensing [12,13] and actuation [14,15] via 3D printing.

Furthermore, 3D-printing technique has been exploited in utilizing transparent polymers to generate functional optical structures such as lenses [16], prisms, and even waveguides [17]. In this manuscript, we summarize our effort in developing a nearly fully 3D-printed confocal imager that can be manufactured at a significantly lowered cost as opposed to its counterparts that are summarized above.

We share the quantitative details behind producing an optical quality lens, a magnetically actuated electromechanical scanner unit, and the housing, which are all 3D printed. Besides offering low-cost fabrication capability of functional opto-mechanical components, 3D printing brings significant advantages into play; Firstly, 3D printing offers deposition of  $\sim 10 \mu\text{m}$  thick layers from which micro-scanners can be produced within  $10 \times 10 \text{ mm}^2$  area that is comparable to the size of off-the-shelf MEMS scanner die size[6,18,19].

Moreover, 3D printing offers manufacturing of arbitrary thickness profile, enabling the production of scanner units having elliptic cross-sectioned mechanical springs [20]. In return, the stress-levels of the electromechanical unit during operation can be significantly reduced. The following sections summarize manufacturing and testing of a 3D-printed lens, 3D-printed scanner, and the housing. Finally we share initial tests on the integrated device, showcasing a lissajous scan on the sample location, and readout from a resolution target.

## 2. FABRICATION OF 3D-PRINTED LENS

### 2.1. Fabrication of 3d-Printed Bulky Lens

We conducted the first set of trials in an attempt to manufacture a bulky (25-mm diameter,  $f = 100$ -mm) plano-convex lens, due to the ease of post-processing (polishing) at this particular size.

The targeted lens was fabricated using a transparent polymeric material (veroclear) with a 3D printer (OBJET Eden 260v) offering  $16\ \mu\text{m}$  printing resolution in the axial direction. The printed lens was then manually polished with a 2000 grade emery polisher, followed by a fine polishing step, where  $\sim 2$ ml of wax-polish (Meguiars M101) was directly applied on the lens via an optical cleaning tissue.

Figure 2.1 and Figure 2.2 illustrates the printed lenses before and after the polishing steps, respectively. The surface profile of both the 3D-printed lenses and an off-the-shelf lens (Thorlabs LA1509) having the same diameter and radius of curvature were acquired using a profilometer (Bruker DektakXT), as illustrated in Figure 2.4. Note that the radius of curvature of both the 3D printed ( $R_{\text{printed}} = 50.5\ \text{mm}$ ) and commercial lens ( $R_{\text{commercial}} = 51.7\ \text{mm}$ ) match to a good extent.

The surface roughness of both lenses were measured through first digitally flattening the surface profile by subtracting a smoothed (moving average filter applied) version of the profiles from the original profiles, and then calculating the root-mean-square (RMS) of the flattened middle 10-mm portion of the lenses.

RMS calculations reveal a surface roughness of 70-nm ( $\sim \lambda/10$ ) and 140-nm ( $\sim \lambda/5$ ) for the commercial lens and the polished 3D-printed lens respectively, indicating only x2 degradation in surface roughness for the 3D printed lens.

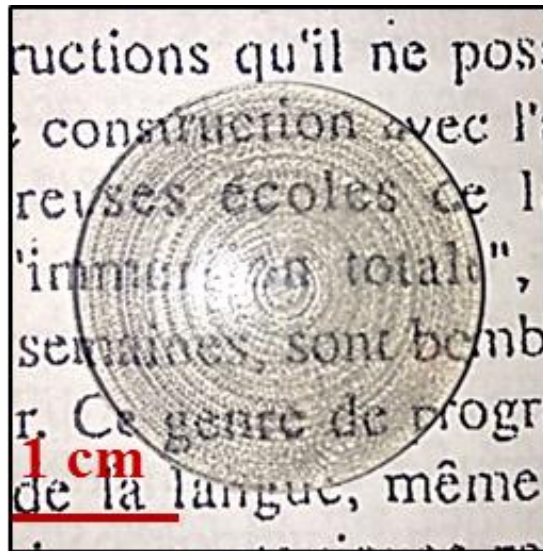


Figure 2.1 : 3D Printed Lens.

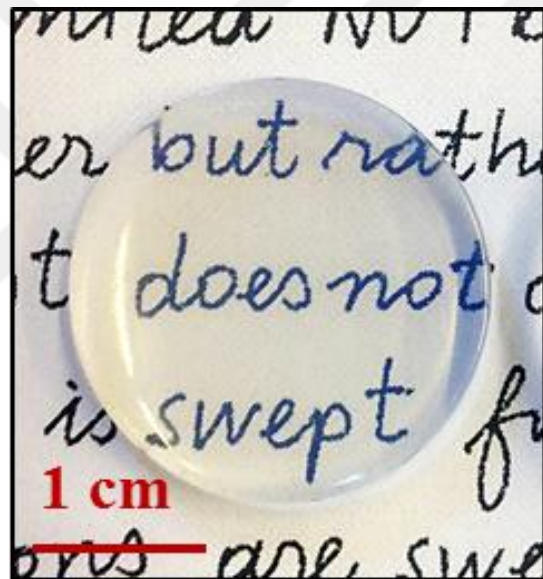
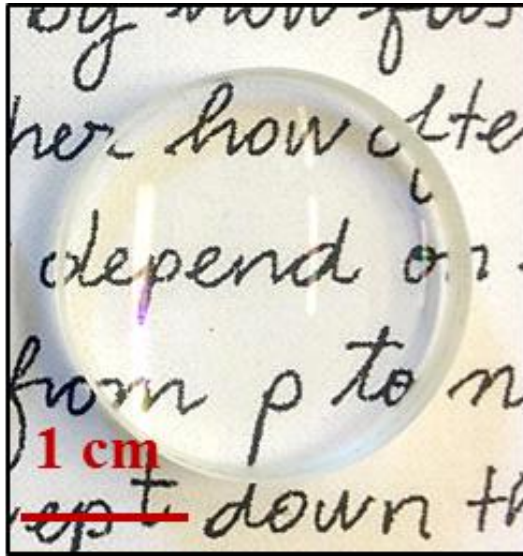
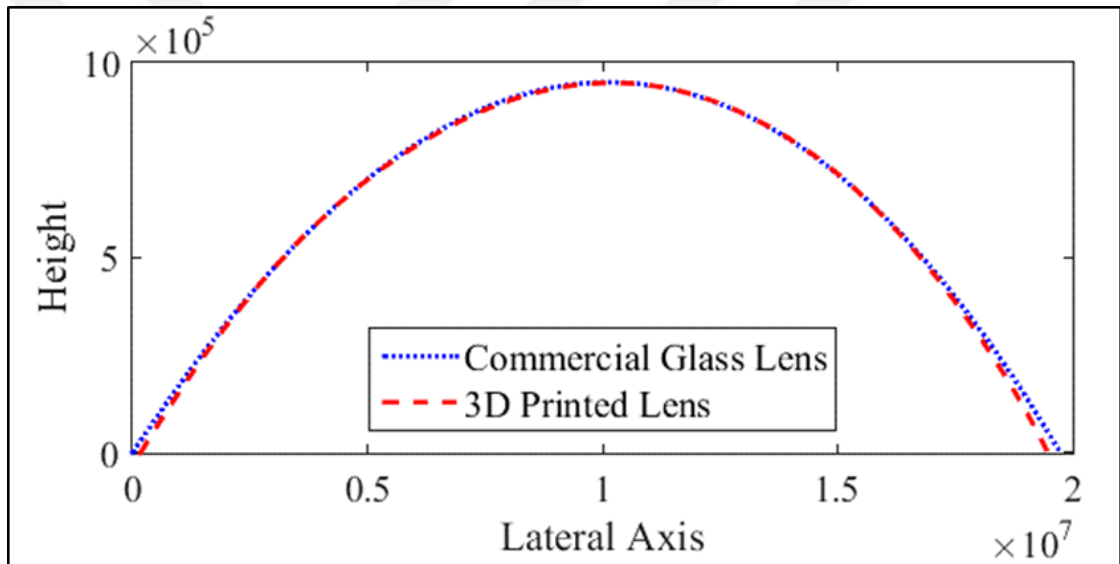


Figure 2.2 : Processed 3D Printed Lens.





**Figure 2.3 :** Commercial Glass Lens



**Figure 2.4 :** Comparison of Lens Surfaces.

The fabrication and surface profiler measurements were followed by focal spot characterization, where a collimated laser beam having ~3-mm diameter was focused onto a CMOS camera via the 3D-printed lens and the reference commercial lens.

The presence of multiple equally spaced focused spots, as illustrated in Figure 2.5, hinted of a periodic diffraction grating-like structure that is inherent within the 3D printed lens.

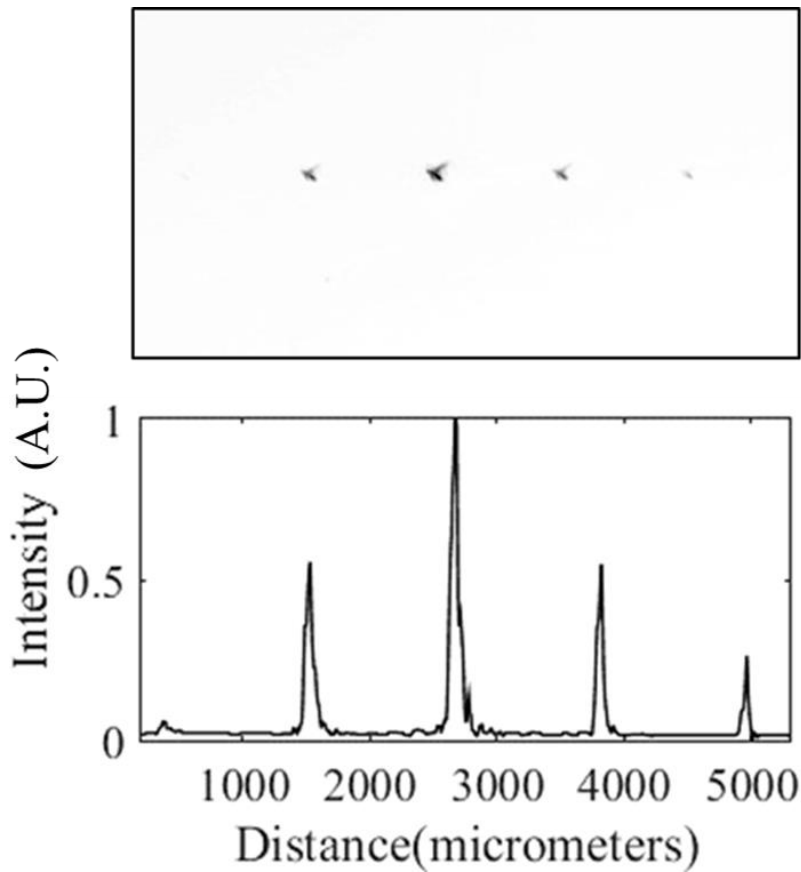


**Figure 2.5.** Lens focus with support (top), illustrating central cross sections of top image (bottom).

Clear investigation of the 3D printing support material (Objet Jumbo Support - FullCure705) revealed a periodic pattern, which can be seen in Figure 2.6, as the source of the diffraction effect, hence we continued our manufacturing efforts by skipping the printing steps of the support material to eliminate the presence of the periodic structure inside the lens.

Without the support material, the focusing experiments resulted in a single focused spot, as illustrated in Figure 2.7.

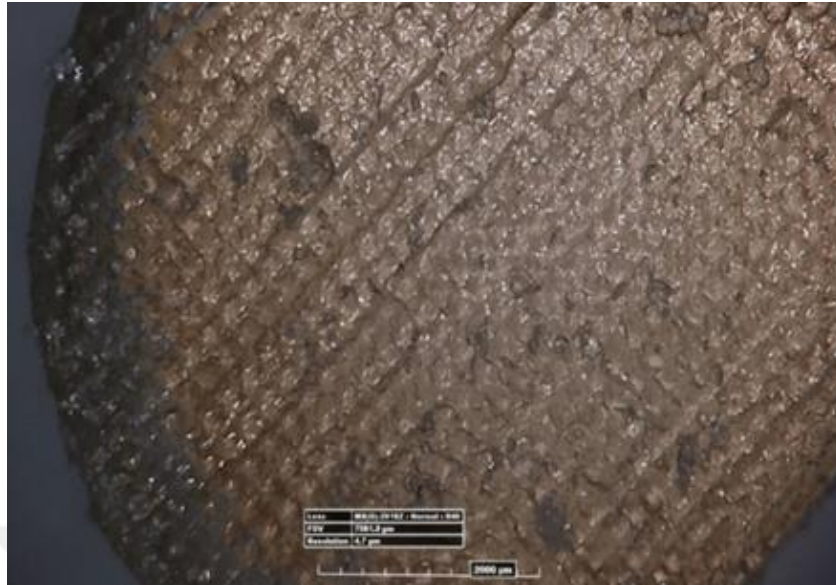


**Figure 2.6.** Periodic Pattern Of Support Structure.

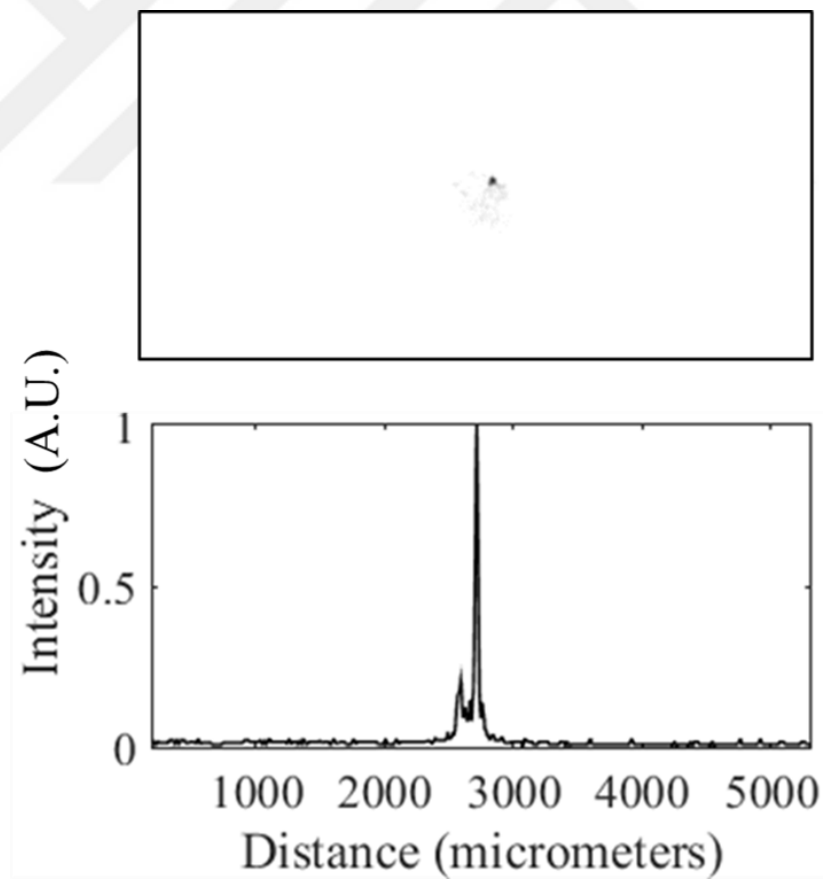


**Figure 2.7.** Lens focus without support (top), illustrating central cross sections of top image (bottom).

## 2.2. Fabrication of the Miniaturized Imager Lens

With the experience gained in manufacturing the bulky lens, we focused our efforts on fabricating a miniaturized plano-convex lens using the same methodology. Figure 2.8 illustrates the printed lens, together with other commercial lenses that were tested.



**Figure 2.8.** i. Commercial 3D Printed Lens, ii.3D Printed Lens (This Work),  
iii.Commercial Glass Lens.

Figure 2.9 illustrates a spot size comparison, acquired through focal spot characterization (Using a 0.85-mm input beam diameter and a telescope setup to x4 magnify the focused spot onto the CMOS camera), of a glass-based commercial lens (Thorlabs LA1116), a 3D-printed commercial lens (Luxexcel Inc.), and our in-house 3D-printed and polished lens having identical diameter (6-mm) and focal length ( $f = 10$ - mm).

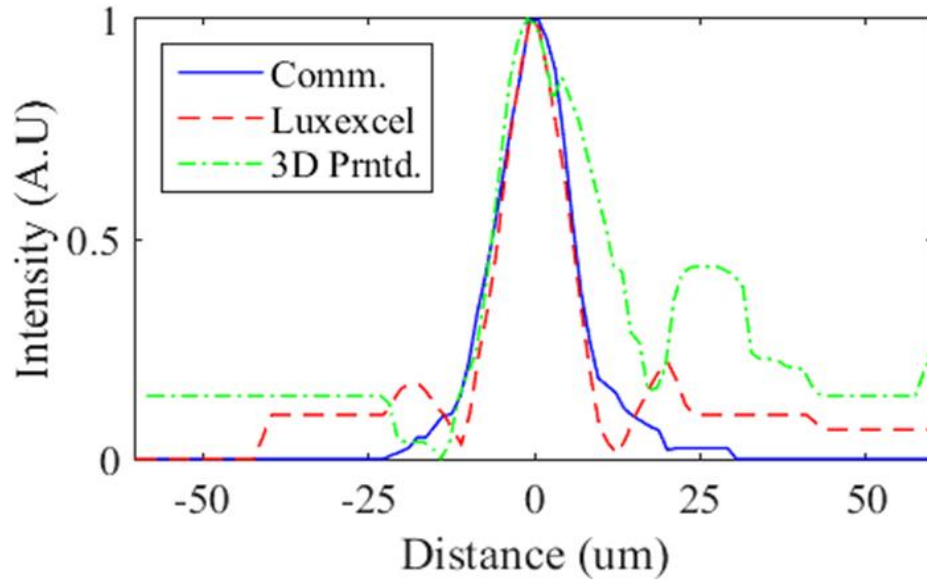


**Figure 2.9.** Spot Comparison Graph of Commercial 3D Printed Lens, 3D Printed Lens (This Work), Commercial Glass Lens.

The focusing tests, revealed a Full-Width Half-Maximum (FWHM) spot size of 12.3  $\mu\text{m}$ , 11.2  $\mu\text{m}$ , and 17.6  $\mu\text{m}$  (The acquired spot size dimensions were multiplied by 0.25 to exclude the effect of the 4x magnifying telescopic setup) for the commercial glass, the 3D printed commercial, and for the in-house 3D printed / polished lenses, respectively.

Although the focusing tests with the miniaturized lenses were performed with an NA of  $\sim 0.05$ , the observed spot sizes were above the diffraction limit, likely due to spherical aberrations. Nevertheless, all three lenses were tested under identical conditions., The in-house 3D printed lens exhibits a wide focused spot along with a significant tail, possibly due to the scattering caused by air gaps in between its printed layers.

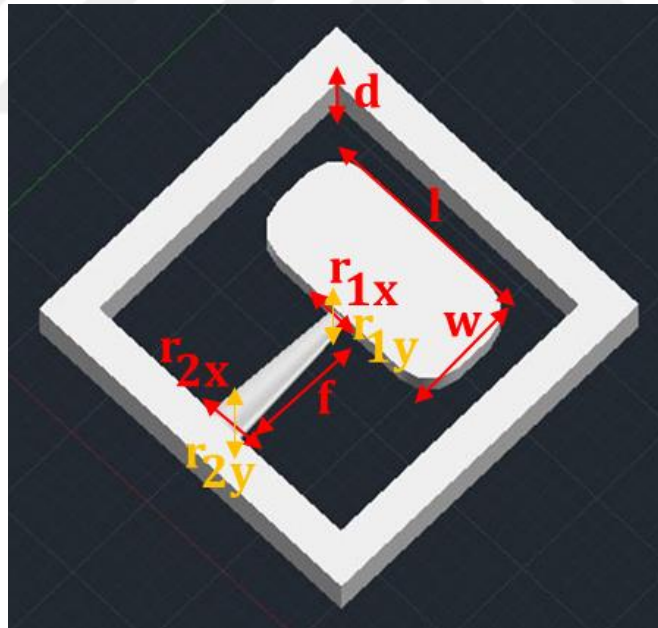
Optimization of the ultraviolet (UV) illumination scheme during 3D printing remains as a possible performance enhancement step to boost the performance of the lens. While our efforts in improving the performance of the 3D in-house printed lens continue, we utilized the 3D printed commercial lens by Luxexcel during the assembly of the imager, to show ultimate performance of a near fully 3D printed system.



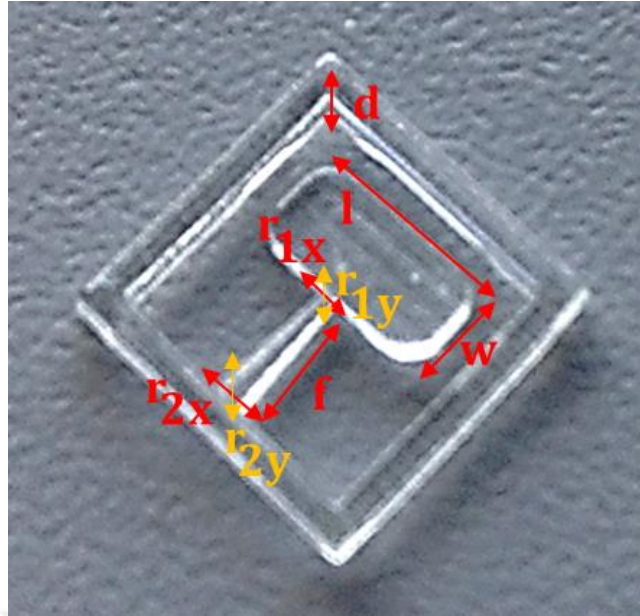
### 3. 3D-PRINTED MICROSCANNER

Figure 3.1 illustrates the design of a 2-D microscanner, having a die area of  $10 \times 10 \text{ mm}^2$ , which is comparable to the size of commercial Silicon MEMS scanners, whose die area typically span  $\sim 5 \times 5 \text{ mm}^2$ . The scanning structure, having  $7 \times 3 \text{ mm}^2$  mirror area and 4-mm long flexure beam, which has an elliptical cross-section, is designed to produce both out-of-plane bending and torsional resonant modes.

Figure 3.2 shows the manufactured scanner out of veroclear material. Through tailoring the mirror and flexure dimensions, together with the flexure taper the first two vibration modes were set as out-of-plane displacement and torsion, while pushing other undesired mechanical modes to higher frequencies and securing a good mode separation. The dimensions of the designed structure are given in Table 3.1.



**Figure 3.1.** CAD Drawing Of The Designed Microscanner Structure.



**Figure 3.2.** The Manufactured Microscanner Structure.

**Table 3.1. :** Dimensions of the scanner.

Section	Size (mm)
d (Depth of the scanner)	1
l (Length of the scanner)	7
w (Width of the scanner)	3
$r_{1x}$ (Major axis (x) radius of the elliptic flexure cross section at the scanner end)	0.25
$r_{1y}$ (Minor axis (y) radius of the elliptic flexure cross section at the scanner end)	0.125
$r_{2x}$ (Major axis (x) radius of the elliptic flexure cross section at the frame end)	0.5
$r_{2y}$ (Minor axis (y) radius of the elliptic flexure cross section at the frame end)	0.25
f (Flexure length)	4

The 3D printing of the scanner unit is followed by its integration with a Cr-Au coated silicon die piece (as the reflective mirror) at the input beam side and a cylindrical (3-mm diameter, 1-mm thickness) neodymium magnet at the actuation side using epoxy glue.



The mechanical frequency response of the scanner is acquired by exciting the scanner via an electrocoil (5-mm diameter, 5- mm height), which is placed at a distance of ~5- mm from the neodymium magnet, and measuring the displacement of the mirror through a Laser Doppler Vibrometer (Polytech LDV) for excitation frequencies between 100 Hz and 600 Hz with 0.5 Hz steps.

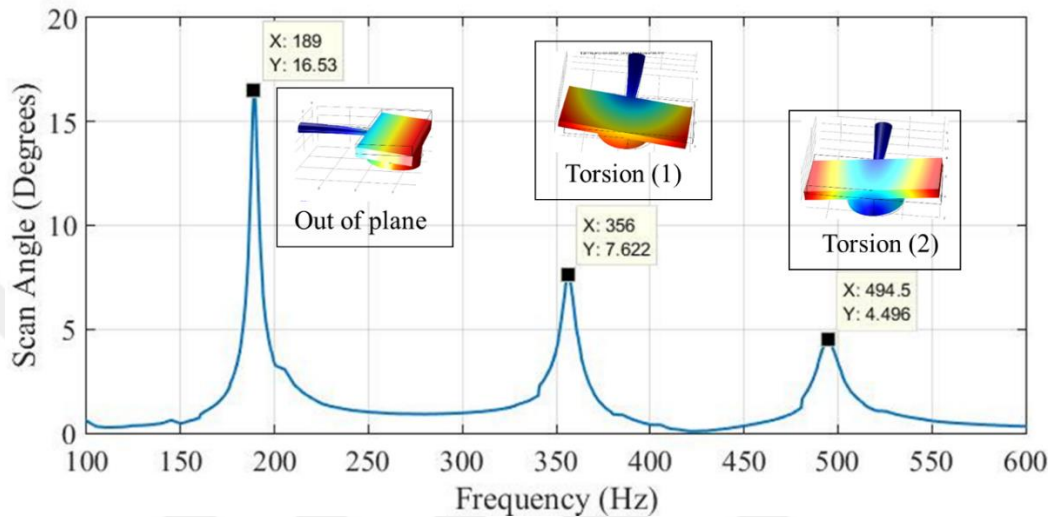


**Figure 3.3.** The Frequency Response Of The 3D Printed Scanner, As Acquired By The LDV Unit. FEM Modal Analysis Results Are Also Included Above Each Corresponding Mode.

A peak-to-peak voltage of 5 V is applied to the coil, drawing 65 mA (rms) of current. Figure 3.3 illustrates the frequency response (scan angle vs. frequency) of the scanner, together with Finite-Element\_Analysis results, showcasing first three vibration modes. The coil was simultaneously driven at the out-of-plane (189 Hz) and torsional (356 Hz) frequencies of the scanner to generate a lissajous scanning pattern. Note that the mode frequencies match-well within 1%, 4% and 15% error to that found from Finite-Element-Analysis software for the first three modes, respectively.

As will be illustrated in the upcoming sections, the scanner is capable of producing a lissajous scan, when out-of-plane and torsion modes are simultaneously excited through driving the coil at the combination of both frequencies. For the first two vibration modes and for the given drive voltage / current, the scanner is able to produce a scan angle of  $\pm 8^\circ$  and  $\pm 4^\circ$ , respectively.

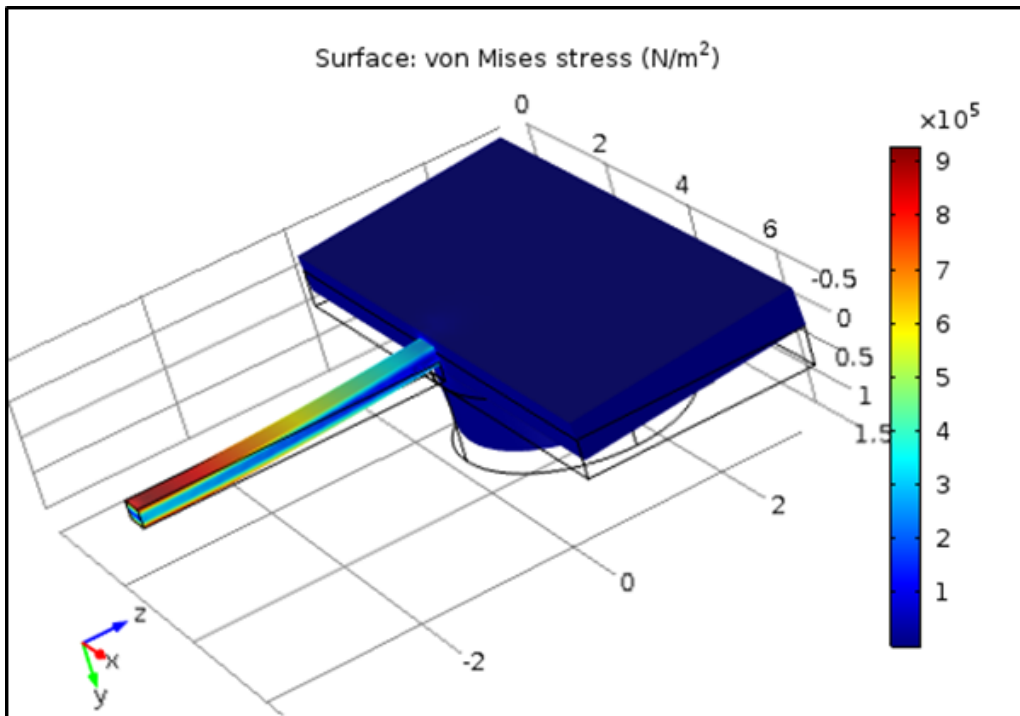


**Figure 3.4.** Von Mises Stress Analysis Of The Rectangular Flexure.

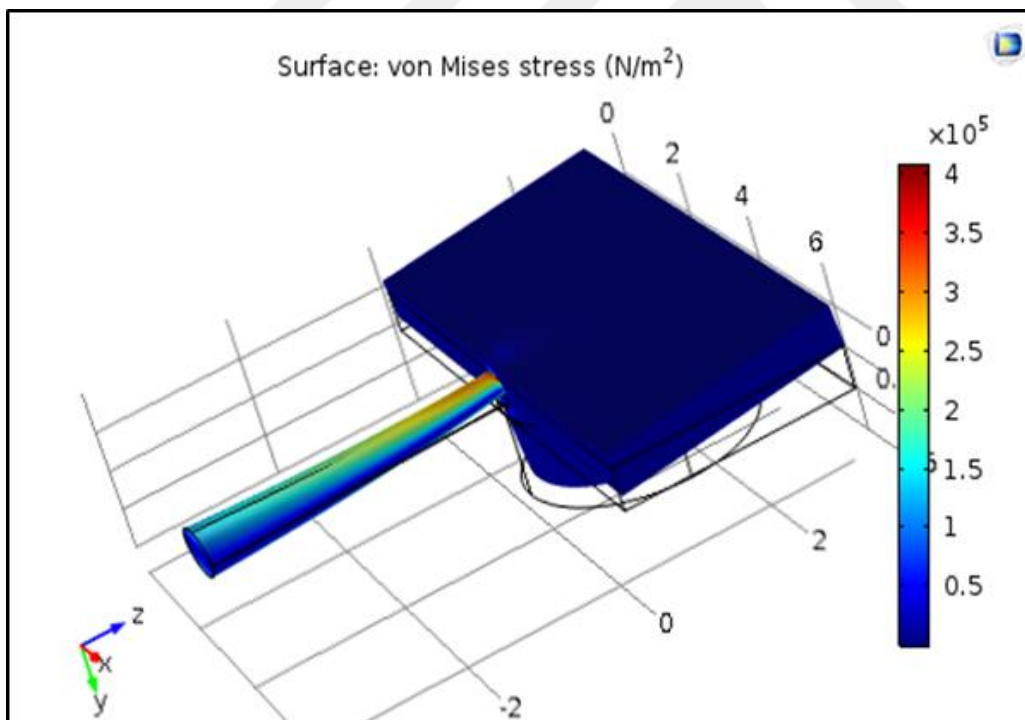


**Figure 3.5.** Von Mises Stress Analysis Of The Elliptic And Tapered Flexure Revealing  
> x2 Times Reduced Stress Levels.

As employed in the designed scanner structure, 3D printing allows for fabricating arbitrary thickness profiles (circular, elliptic, etc.) that can be used for releasing the stress from the flexure joints.

Figure 3.4 and Figure 3.5 compares the von Mises stress levels of two similar scanner structures showcasing similar resonance behaviour.

The scanner shown in Figure 3.5 has an elliptic flexure cross section and the other scanner which is shown in Figure 3.4 has a rectangular flexure cross section.

The scanner with elliptic flexure cross section reveals  $> \times 2$  reduction in the stress levels when compared with the rectangular cross-sectioned scanner.

Thus, owing to 3D printing technology the elliptic flexure profile not only allows for mode separation between out-of-plane bending and in-plane sliding modes, but also significantly reduces the accumulated stress during dynamic operation.

Stress reduction plays an important role on the reliability of the scanner for higher stress causes more fragile structures.



#### 4. 3D-PRINTED HOUSING, SYSTEM INTEGRATION AND CHARACTERIZATION

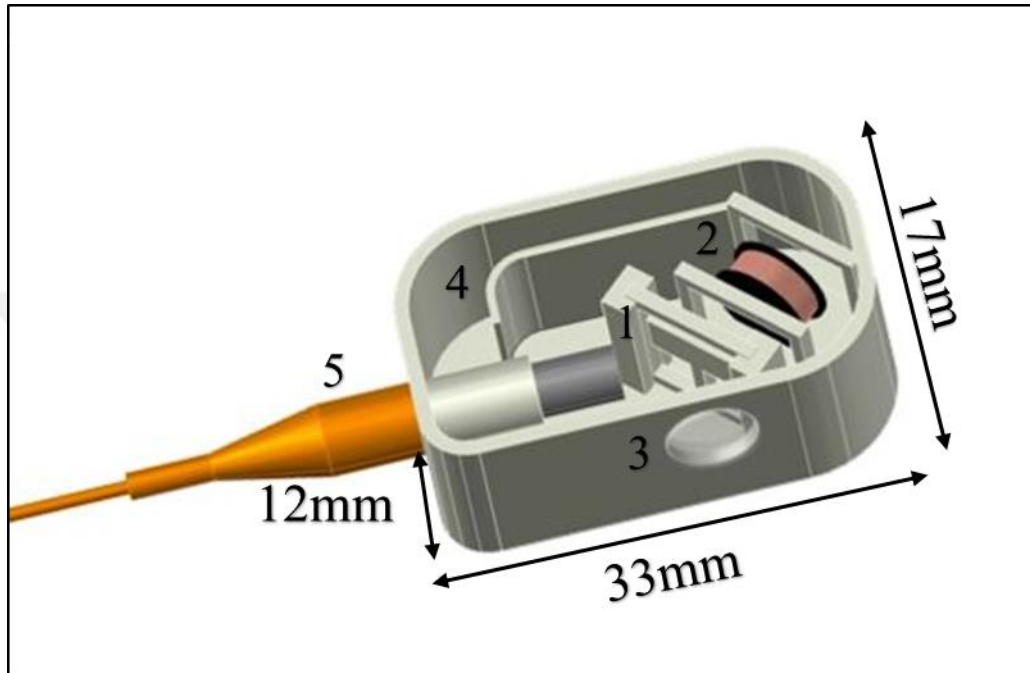


**Figure 4.1.** The Housing Unit in Which The Components Are Assembled CAD Drawing. The Shown Components Are: 1) Scanner, 2) Coil, 3) Lens, 4) Electrical Interconnect Channel, 5) Input Fiber

Figure 4.1 illustrates the 33-mm x 17-mm x 12-mm (width x length x thickness) sized housing design to encapsulate the scanner and the lens. A hollow cavity of 3.2-mm diameter is dedicated for the input GRIN collimated single-mode fiber assembly (Thorlabs 50-630-FC) that delivers the laser light to the scanner. The input single-mode fiber also acts as a pinhole for acquiring confocal images.

Multiple grooves are dedicated for the microscanner, electro coil, and the miniaturized lens. The 5-mm distance between the coil and the scanner (same distance that was deployed in characterizing the scanner alone) is optimized to maintain adequate amount of actuation force, while preventing contact between the neodymium magnet that is located on the scanner and the coil.

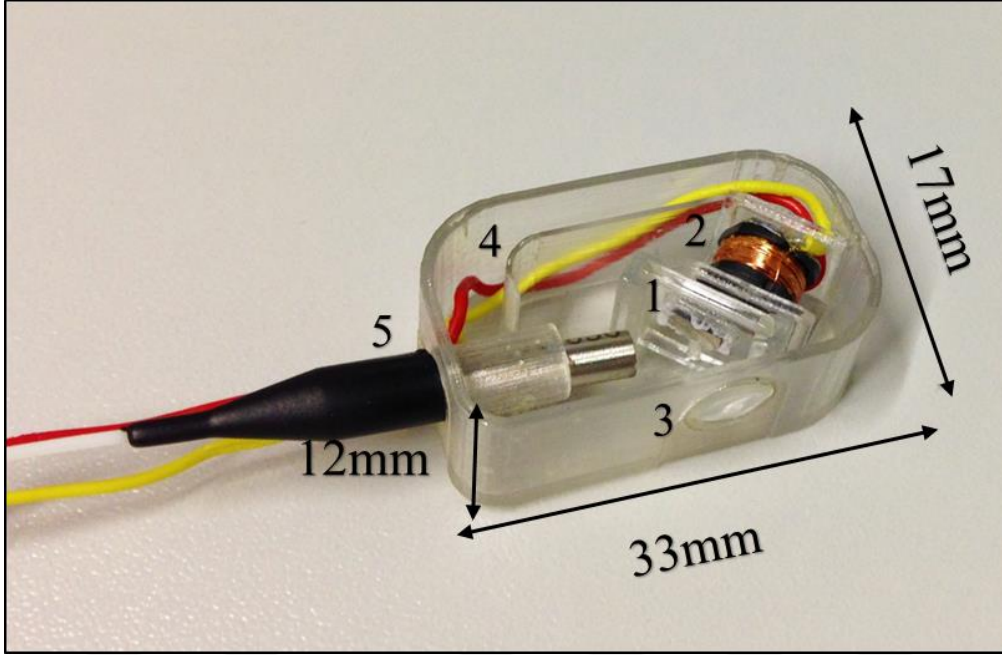


**Figure 4.2.** The Housing Unit in Which The Components Are Assembled Photo Of The Manufactured Unit. The Shown Components Are: 1) Scanner, 2) Coil, 3) Lens, 4) Electrical Interconnect Channel, 5) Input Fiber

A channel, located on the opposite side of the lens, is reserved for the electrical interconnects to the coil. Figure 4.2 showcases the 3D printed housing. All constituents (input fiber, scanner, coil, miniaturized lens) are press-fit into their corresponding grooves.

Considering a beam size of 0.85-mm diameter, which is underfilling the focusing lens, for the GRIN collimated single-mode fiber, the miniaturized lens provides an effective numerical aperture (NA) of 0.043, while sparing most of the 3D printed lens aperture for the beam scanning to produce a large FOV.

With the given NA and for the input wavelength of  $\lambda = 630\text{-nm}$ , the focused FWHM spot size ( $\delta xy$ ) is estimated a  $7\text{-}\mu\text{m}$  based on the equation below, offering cellular level resolution [21].

$$\delta xy \approx \lambda / 2NA \quad (4.1)$$

The FOV could be calculated based on the product of zero-to-peak optical scan angle ( $\theta$ , in radians) with the objective lens focal length ( $f$ ) such that [4]:

$$FOV = 2\theta f \quad (4.2)$$

Based on the acquired scan angles of  $\pm 8^\circ$  and  $\pm 4^\circ$ , for the first two mechanical modes, at 5V drive voltage, we expect a FOV of  $\sim 2.8 \times 1.4 \text{ mm}^2$  in the assembled system. Since the housing does not incorporate means to optimize the electrocoil position with respect to the scanner, we expect a smaller FOV in the assembled system.

Yet, through increasing the drive voltage or optimizing the electro-coil position in the assembly, one can reach the desired FOV.

Furthermore, a square-shaped FOV may be obtained by applying different voltages to different axes. Note that the resolution could be significantly improved by the use of a larger diameter input beam through introducing a relay lens pair in the system architecture.

However, the relay lens pair would diminish the scan angle on the objective lens (inversely proportional with the amount of magnification introduced by the relay pair), compromising the FOV[4]. The resolution vs. FOV trade-off should be treated based on the requirements of the targeted application.

After successful integration of all optical and mechanical components with the housing, the assembled system was tested using the setup illustrated in Figure 4.3.

A laser diode (Thorlabs CPS196 ) having 635 nm emission wavelength and 1 mW power was coupled into a GRIN collimated single mode fiber (Thorlabs 50-630-FC), which was inserted into the manufactured housing, using a 0.25 NA objective lens.

After impinging the 3D printed scanner, getting focused onto the target via the 3D printed lens, the reflected light beam was recoupled into the fiber and was collected on a photodetector unit (Thorlabs PDA36A) whose intensity output was monitored through an oscilloscope (Tektronix MSO4104).

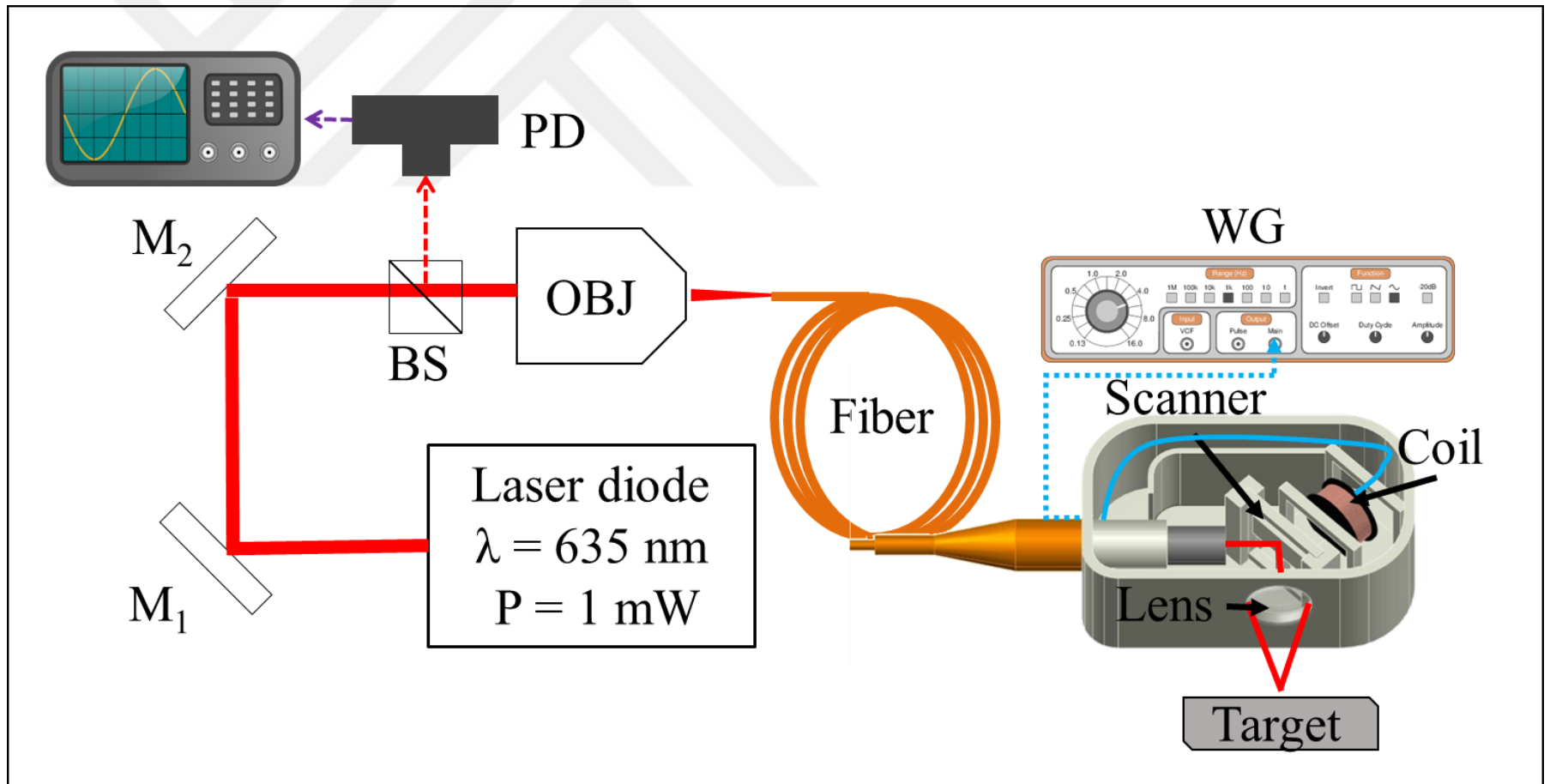


**Figure 4.3.** Characterization Setup ( $M_1, M_2$  : Mirrors, BS : Beam Splitter, PD : Photodetector, OBJ : Objective Lens, WG : Waveform Generator) Used In Acquiring Line Scans From The Target.



The coil was simultaneously driven at the out-of-plane (180 Hz) and torsional (315 Hz) frequencies of the scanner to generate a lissajous scanning pattern, which was observed with a CMOS camera that was placed at the focus of the miniaturized lens, as illustrated in Figure 4.3.

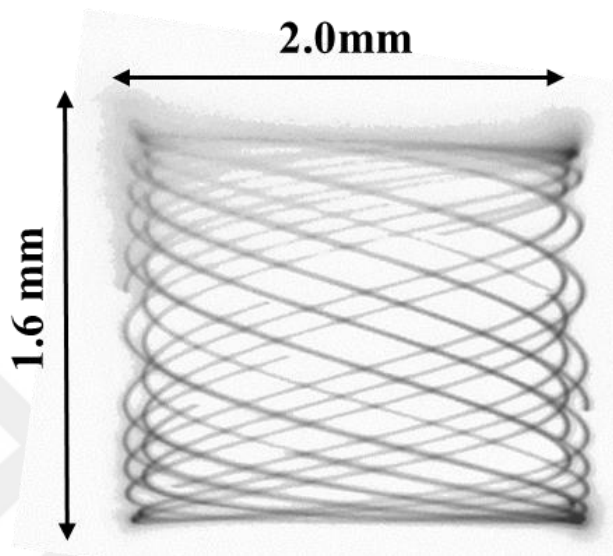


**Figure 4.4.** Lissajous Scan Pattern of the 3D Printed & Miniaturized Confocal Imager.

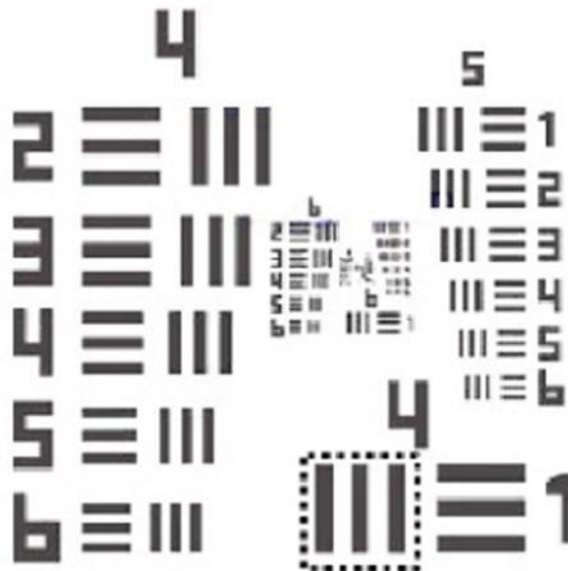


**Figure 4.5** USAF 1951 Resolution Target (4th Group 1st Element Marked in Box).

Since a different scanner unit was integrated inside a housing, apart from that used in the stand-alone scanner characterization the resonant frequencies were observed to be slightly different than the ones shown in Figure 3.3.

The coverage of the lissajous pattern can be improved through slightly varying the frequencies to mutually prime values, at the expense of reduced frame-rate [22].

The image of the scanning pattern reveals a FOV of 1.6-mm x 2-mm for a peak-to-peak drive voltage of 30 and 50 Volts for 1st and 2nd mechanical resonances respectively. Note that the drive voltages can be significantly reduced with optimized electro-coil position.

As mentioned earlier, the higher voltage requirement arose due to sub-optimal electro coil placement, which could be reduced through tailoring the position of groove that was dedicated for the coil.

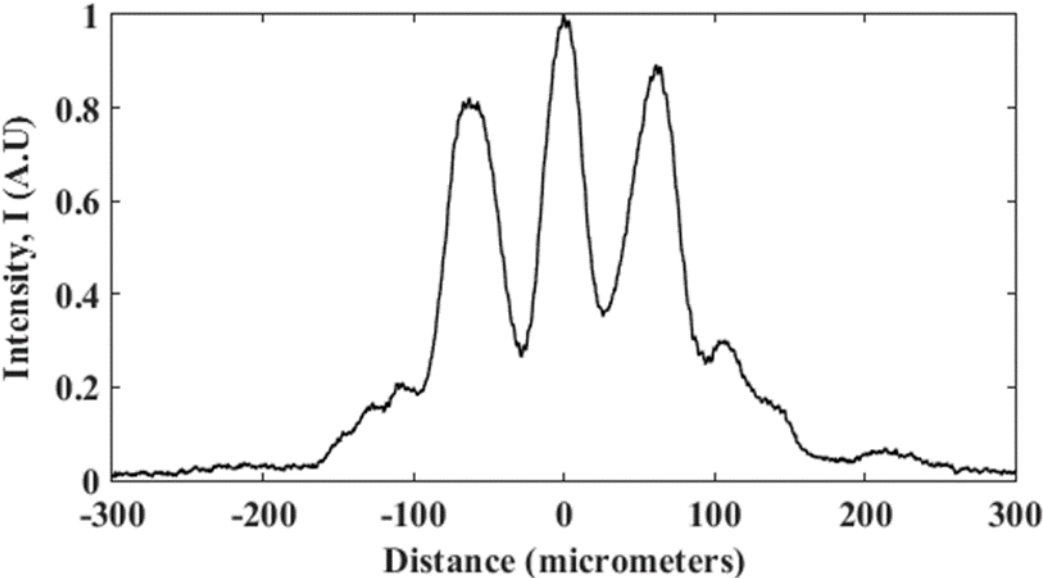


**Figure 4.6** The Distance-Intensity (I) Graph Acquired From the 4th Group 1st Element

Figure 4.6 further illustrate the USAF target pattern on which a line scan is taken by the integrated confocal imager (Group 4 element 1), showcasing the capability of comfortably distinguishing 30- $\mu\text{m}$  stripes.

Figure 4.7 illustrates the spatial derivative of the resolution target reading (step-function profile), revealing the spot size [23] that is found as 11.4- $\mu\text{m}$ , which is higher than the theoretically found value of 7-  $\mu\text{m}$ .

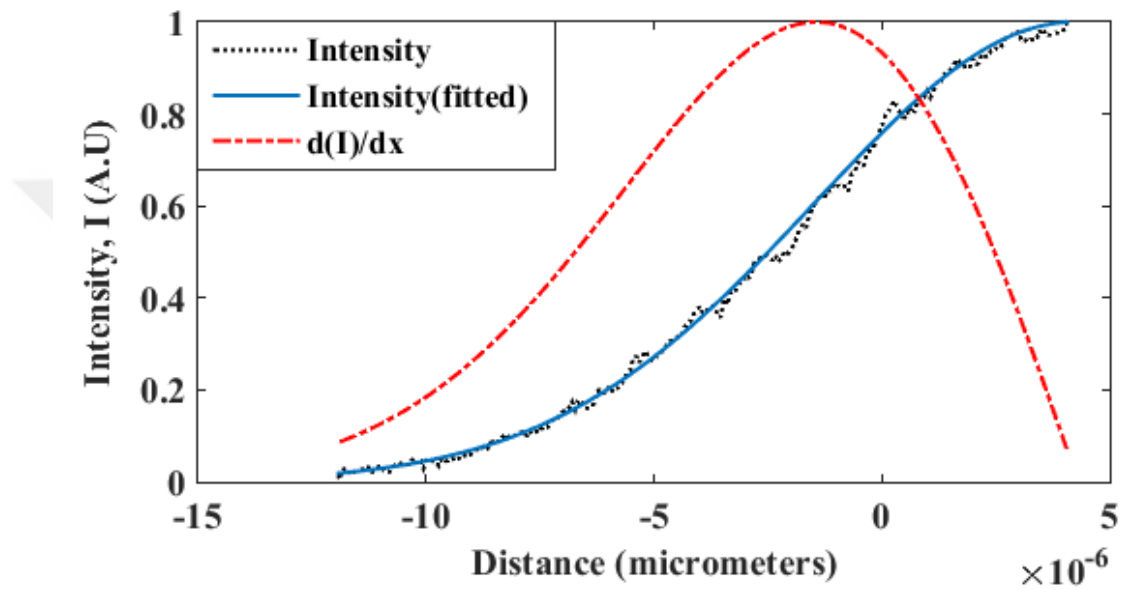


**Figure 4.7** Close-Up View of the First Step Showing in Fig 4.7, And Its Spatial Derivative That Reveals A FWHM Resolution Of 11.4- $\mu\text{m}$ .

We attribute the difference to the spherical aberrations that is introduced by the lens. Note that the measured FWHM resolution of 11.4- $\mu\text{m}$  matches the resolution observed in the stand-alone focusing experiments of the miniaturized lenses (11.2  $\mu\text{m}$ , with identical NA) that was performed under identical conditions.



## 5. CONCLUSIONS AND DISCUSSION

A miniaturized confocal imager is presented, consisting of 3D printed functional optical and electromechanical parts, such as the lens and the microscanner, together with the housing. 3D printed lens and the microscanner were thoroughly characterized, showcasing promising performance when compared to glass-lens and MEMS scanner counterparts at a much lower cost.

Furthermore, 3D printing provided a non-planar processing capability for mechanically moving parts, such as the scanner, where the flexures could be built with elliptic cross-sections to release stress during motion.

The prototype was assembled through press fitting of the 3D-printed optical and electromechanical components into the 3D printed housing, where a 2D lissajous scanning capability and acquisition of line scans for a given target were demonstrated.

The manufactured confocal imager required some non-3D-printed parts besides the input GRIN collimated single mode fiber assembly, namely an electro-coil for excitation, a magnet that is placed on the rear side of the microscanner for electromagnetic actuation, and a reflective silicon piece that is placed on the front surface of the microscanner.

Recent advances in the 3D printing technology on i) manufacturing 3D printed electronics, including solenoid inductors through the combination of a 3D printed molds and silver ink [24] ii) manufacturing magnetic materials through mixing Fe<sub>3</sub>O<sub>4</sub> particles with 3D printing powder [25] reveal that even the electro-coil and the magnet components in our imager could be potentially replaced with 3D printed counterparts, almost making the entire design fully-3D printed.

**Table 5.1** Comparison with Similar Studies

Reference	Actuation Voltage	Field of View	Resolution	Size (mm)	Frame Rate (Per Second)
[27]	20 V	$\pm 100 \mu\text{m}$ .	$1.3 \mu\text{m}$	$165 \times 45 \times 40$	NA
[28]	3V	$2.85 \text{ mm} \times 2.85 \text{ mm}$	$10.6 \mu\text{m} \times 17.5 \mu\text{m}$	$5 (\varnothing)$	50 fps
[29]	NA	NA	$30 \mu\text{m} \times 7 \mu\text{m}$	$24.8 (\text{length}) \times 12.8 (\varnothing)$	20 fps
[30]	No actuation required	$660 \mu\text{m}$	$5.0 \mu\text{m}$	$800 \mu\text{m}$ (fiber bundle)	4 fps
[31]	$\pm 20$ volts	$200 \mu\text{m}$	$0.98 \pm 0.09 \mu\text{m} \times 7.68 \pm 1.30 \mu\text{m}$	1	NA
[32]	80 V	$310 \mu\text{m}$	$1.64 \mu\text{m} \times 16.4 \mu\text{m}$	$10 \times 15 \times 40$	10 fps
[33]	45 V	from $390 \mu\text{m}$ to $655 \mu\text{m}$	$1.27 \mu\text{m} \times 13.5 \mu\text{m}$	$9.6 (\varnothing)$	7 fps
This Work	80 V	$2 \times 1.6 \text{ mm}$	$11.2 \mu\text{m}$	$33 \times 17 \times 12$	45 fps

The developed 17-mm wide confocal imager is comparable in size to many of the MEMS based laser scanning probes that are encountered in literature [4,26].

As seen in Table 5.1, the proposed system makes it well suited for its application onto the skin and open surgical sites, while its invasive use through the gastrointestinal track requires further miniaturization. Furthermore, the proposed imager could be built at a significantly lower price than its counterparts.

Reliability of the 3D printed scanning unit is currently being tested for plastic deformation and spring softening effects, yet these issues are uncritical for a unit that is targeted for disposable use due to low cost polymer material.

With further advances in the 3D printing technology such as the invention of magnetic polymer and the advancing techniques in the use of silver ink, more compact laser scanning probes can be built with higher percentile of 3D printed functional components and even in single printing attempt, making the imager a disposable and low-cost diagnostic tool for clinical use.





## REFERENCES

- [1] **Lee C M, Engelbrecht C J, Soper T D, Helmchen F and Seibel E J** 2010 “Scanning fiber endoscopy with highly flexible, 1 mm catheterscopes for wide-field, full-color imaging” *J. Biophotonics* 3 385–407
- [2] **Xi J, Chen Y, Zhang Y, Murari K, Li M-J and Li X** 2012 “Integrated multimodal endomicroscopy platform for simultaneous en face optical coherence and two-photon fluorescence imaging” *Opt. Lett.* 37 362
- [3] **Zhang Y, Akins M L, Murari K, Xi J, Li M-J, Luby-Phelps K, Mahendroo M and Li X** 2012 “A compact fiber-optic SHG scanning endomicroscope and its application to visualize cervical remodeling during pregnancy” *Proc. Natl. Acad. Sci.* 109 12878–83
- [4] **Hoy C L, Ferhanoglu O, Yildirim M, Piyawattanametha W, Ra H, Solgaard O and Ben-Yakar A** 2011 “Optical design and imaging performance testing of a 9.6-mm diameter femtosecond laser microsurgery probe.” *Opt. Express* 19 10536–52
- [5] **Shin D, Pierce M C, Gillenwater A M, Williams M D and Richards-Kortum R R** 2010 “A fiber-optic fluorescence microscope using a consumer-grade digital camera for in vivo cellular imaging” *PLoS One*
- [6] **Yalcinkaya A D, Urey H, Brown D, Montague T and Sprague R** 2006 “Two-Axis Electromagnetic Microscanner for High Resolution Displays” *J. Microelectromechanical Syst.* 15 786–94
- [7] **Baran U, Brown D, Holmstrom S, Balma D, Davis W O, Muralt P and Urey H** 2012 “Resonant PZT MEMS scanner for high-resolution displays” *J. Microelectromechanical Syst.* 21 1303–10
- [8] **Suter M J, Gora M J, Lauwers G Y, Arnason T, Sauk J, Gallagher K A, Kava L, Tan K M, Soomro A R, Gallagher T P, Gardecki J A, Bouma B E, Rosenberg M, Nishioka N S and Tearney G J** 2014 “Esophageal-guided biopsy with volumetric laser endomicroscopy and laser cautery marking: A pilot clinical study” *Gastrointest. Endosc.* 79 886–96
- [9] **Murari K, Zhang Y, Li S, Chen Y, Li M-J and Li X** 2011 “Compensation-free, all-fiber-optic, two-photon endomicroscopy at 1.55  $\mu\text{m}$ .” *Opt. Lett.* 36 1299–301
- [10] **Ferhanoglu O, Yildirim M, Subramanian K and Ben-Yakar A** 2014 “A 5-mm piezo-scanning fiber device for high speed ultrafast laser microsurgery.” *Biomed. Opt. Express* 5 2023–36

- [11] **Wu S-Y, Yang C, Hsu W and Lin L** 2015 “3D-printed microelectronics for integrated circuitry and passive wireless sensors” *Microsystems Nanoeng.* 1 15013
- [12] **Shemelya C, Cedillos F, Aguilera E, Maestas E, Ramos J, Espalin D, Muse D, Wicker R and MacDonald E** 2013 “3D printed capacitive sensors” *IEEE SENSORS 2013 - Proceedings*
- [13] **Peele B N, Wallin T J, Zhao H and Shepherd R F** 2015 “3D printing antagonistic systems of artificial muscle using projection stereolithography.” *Bioinspir. Biomim.* 10 055003
- [14] **Ishiguro Y and Poupyrev I** 2014 “3D printed interactive speakers” *Proc. 32nd Annu. ACM Conf. Hum. factors Comput. Syst. - CHI '14* 1733–42
- [15] **Debellemanni G, Flores M, Montard M, Delbosc B and Saleh M** 2016 “Three-dimensional Printing of Optical Lenses and Ophthalmic Surgery: Challenges and Perspectives” *J. Refract. Surg.* 32 201–4
- [16] **Willis K, Brockmeyer E, Hudson S and Poupyrev I** 2012 “Printed optics: 3D printing of embedded optical elements for interactive devices” *Proc. 25th Annu. ACM Symp. User interface Softw. Technol. - UIST '12* 589–98
- [17] **Milanović V, Matus G A and McCormick D T** 2004 “Gimbal-less monolithic silicon actuators for tip-tilt-piston micromirror applications” *IEEE J. Sel. Top. Quantum Electron.* 10 462–71
- [18] **Schenk H, Dürr P, Haase T, Kunze D, Sobe U, Lakner H and Kück H** 2000 “Large deflection micromechanical scanning mirrors for linear scans and pattern generation” *IEEE J. Sel. Top. Quantum Electron.* 6 715–22
- [19] **Oyman A, Gokdel Y D, Ferhanoglu O and Yalcinkaya A D** 2016 “3D Printed MEMS Micro-Scanner for Laser Scanning Endoscopy” *Sensors Actuators A Phys.* (submitted)
- [20] **Urey H** 2004 Spot size, depth-of-focus, and diffraction ring intensity formulas for truncated Gaussian beams. *Appl. Opt.* 43 620–5
- [21] **Hoy C L, Durr N J and Ben-Yakar A** 2011 “Fast-updating and nonrepeating Lissajous image reconstruction method for capturing increased dynamic information.” *Appl. Opt.* 50 2376–82
- [22] **Ouzounov D G, Rivera D R, Webb W W, Bentley J and Xu C** 2013 “Miniature varifocal objective lens for endomicroscopy” *Opt. Lett.* 38 3103
- [23] **Yang C, Wu S-Y, Glick C, Choi Y S, Hsu W and Lin L** 2015 “3D printed RF passive components by liquid metal filling” 2015 28th IEEE Int. Conf. Micro Electro Mech. Syst. 261–4
- [24] **Zhang J H, Zhao S C, Zhu M, Zhu Y F, Zhang Y D, Liu Z T and Zhang C Q** 2014 “3D-printed magnetic Fe<sub>3</sub>O<sub>4</sub>/MBG/PCL composite scaffolds with

multifunctionality of bone regeneration, local anticancer drug delivery and hyperthermia" *J. Mater. Chem. B* 2 7583–95

[25] **Piyawattanametha W, Cocker E D, Burns L D, Barretto R P, Jung J C, Ra H, Solgaard O and Schnitzer M J** 2009 "In vivo brain imaging using a portable 2.9 g two-photon microscope based on a microelectromechanical systems scanning mirror." *Opt. Lett.* 34 2309–11

[26] **Yuan Zhao, Mingyu Sheng, Lin Huang, and Shuo Tang**, 2016 "Design of a fiber-optic multiphoton microscopy handheld probe," *Biomed. Opt. Express* 7, 3425-3437

[27] **Duan, C., Zhang, X., Wang, D., Zhou, Z., Liang, P., Pozzi, A. and Xie, H.** 2014. An endoscopic forward-viewing OCT imaging probe based on a two-axis scanning mems mirror. 2014 IEEE 11th International Symposium on Biomedical Imaging (ISBI).

[28] **Gora, M., Sauk, J., Carruth, R., Gallagher, K., Suter, M., Nishioka, N., Kava, L., Rosenberg, M., Bouma, B. and Tearney, G.** 2013. Tethered capsule endomicroscopy enables less invasive imaging of gastrointestinal tract microstructure. *Nature Medicine*, 19(2), pp.238-240.

[29] **Shin, D., Pierce, M., Gillenwater, A., Williams, M. and Richards-Kortum, R.** 2010. A Fiber-Optic Fluorescence Microscope Using a Consumer-Grade Digital Camera for In Vivo Cellular Imaging. *PLoS ONE*, 5(6), p.e11218.

[30] **Lee, C., Engelbrecht, C., Soper, T., Helmchen, F. and Seibel, E.** 2010. Scanning fiber endoscopy with highly flexible, 1 mm catheterscopes for wide-field, full-color imaging. *Journal of Biophotonics*, 3(5-6), pp.385-407.

[31] **Christopher L. Hoy, Nicholas J. Durr, Pengyuan Chen, Wibool Piyawattanametha, Hyejun Ra, Olav Solgaard, and Adela Ben-Yakar**, 2008 "Miniaturized probe for femtosecond laser microsurgery and two-photon imaging," *Opt. Express* 16, 9996-10005.

[32] **Christopher L. Hoy, Onur Ferhanoglu, Murat Yildirim, Wibool Piyawattanametha, Hyejun Ra, Olav Solgaard, and Adela Ben-Yakar**, 2011 "Optical design and imaging performance testing of a 9.6-mm diameter femtosecond laser microsurgery probe," *Opt. Express* 19, 10536-10552.



## **APPENDICES**

### **APPENDIX A: A Guide to 3D Printing**



## APPENDIX A

### A Guide To 3D Printing

3D printing, refers to processes used to create a 3D object in which layers of material are formed under computer control to create an object. It consists of three main steps which are the following:

1. Modeling
2. Printing
3. Finishing



**Figure A.1:** 3D Printing Steps.

#### A.1. Modeling

Modeling for 3D printing is acquired with CAD drawing softwares such as AutoCAD, Solidworks, Sketch-up, Rhinoceros 3D, etc.

In this work AutoCAD software is used. In figure A.2 a screenshot is given. For all pieces were press-fitted, 0.1-0.2 mm gap between the pieces was left as the tolerance.

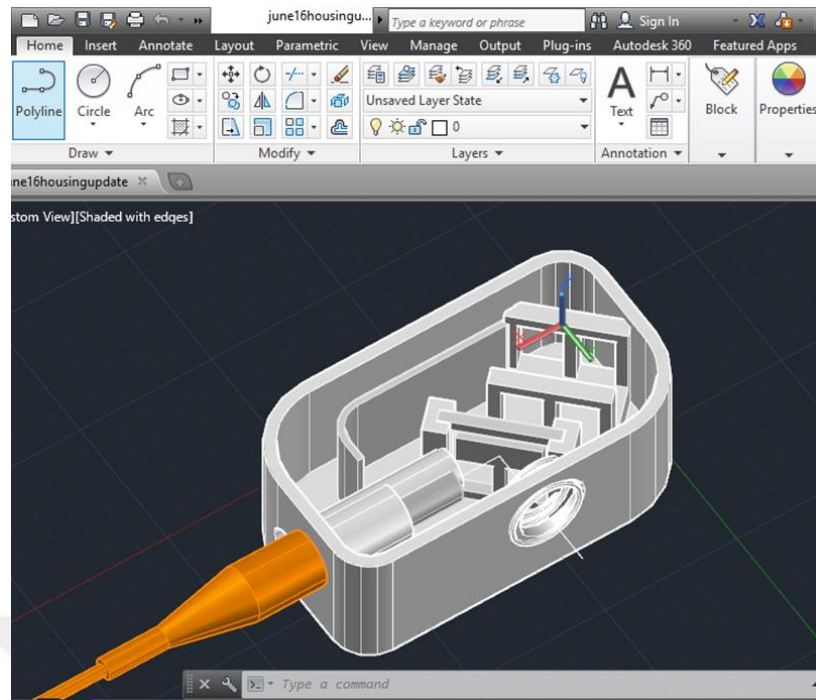


**Figure A.2:** AutoCAD Interface.

When the modeling is finished, the pieces must be unionized and an “.stl” format export should be taken from the export menu.

The format “.stl” stands for STereoLithography but it also has several after-the-fact backronyms such as "Standard Triangle Language" since the file is broken down into a mesh including many triangle pieces.

## **A.2. Printing**

In this particular work Objet260 Connex 3D Printer was used. However most modern commercial 3D Printers follow similar procedures.



**Figure A.3:** Objet260 Connex 3D Printer.

Starting the software of the printer is the first step. The software offers a virtual version of 3D printer's tray seen in Figure A.3 and CAD models can be placed on this virtual tray.

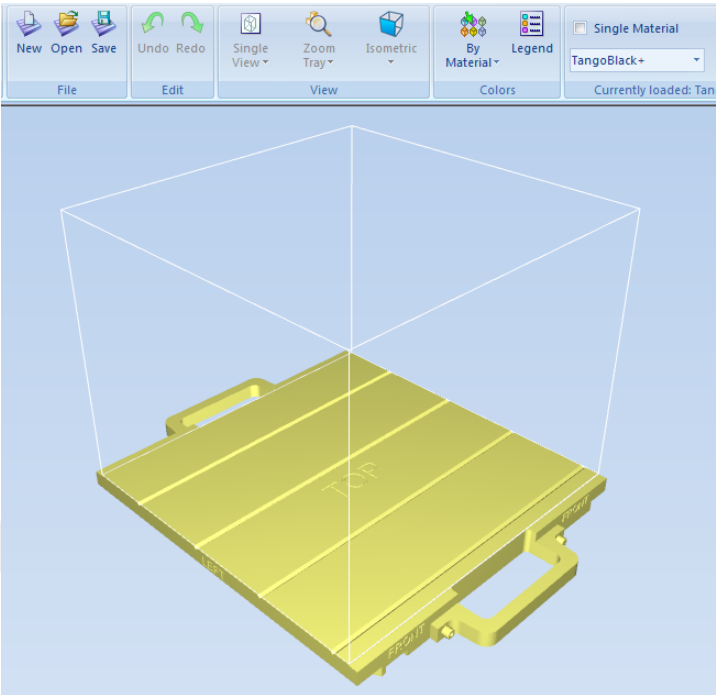


Figure A.4: Objet Studio's Interface and the Tray.

According to the desired properties, position and orientation of the models can be manipulated. Figure A.5 shows the translation, rotation and scale settings.

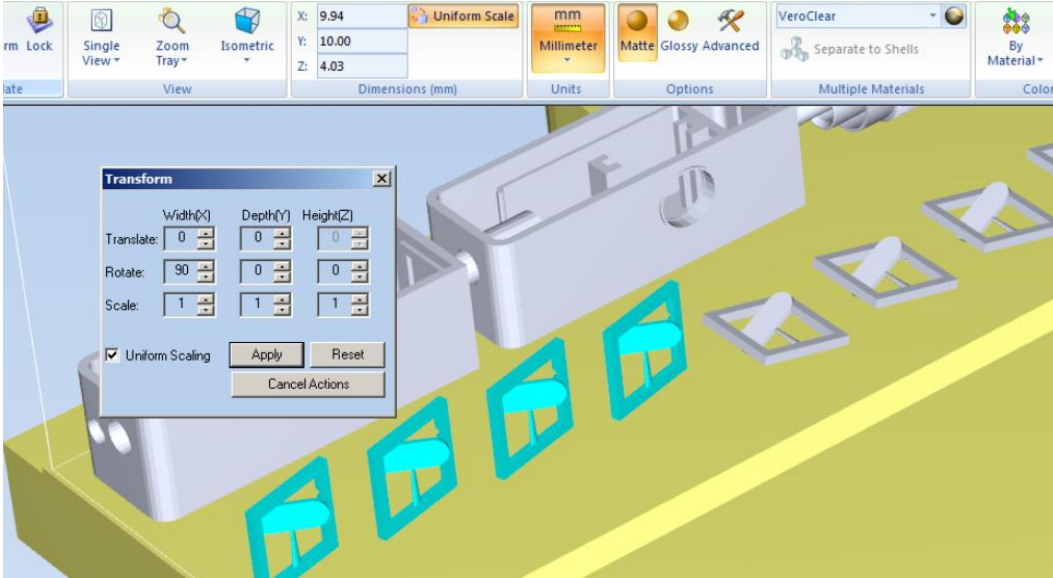
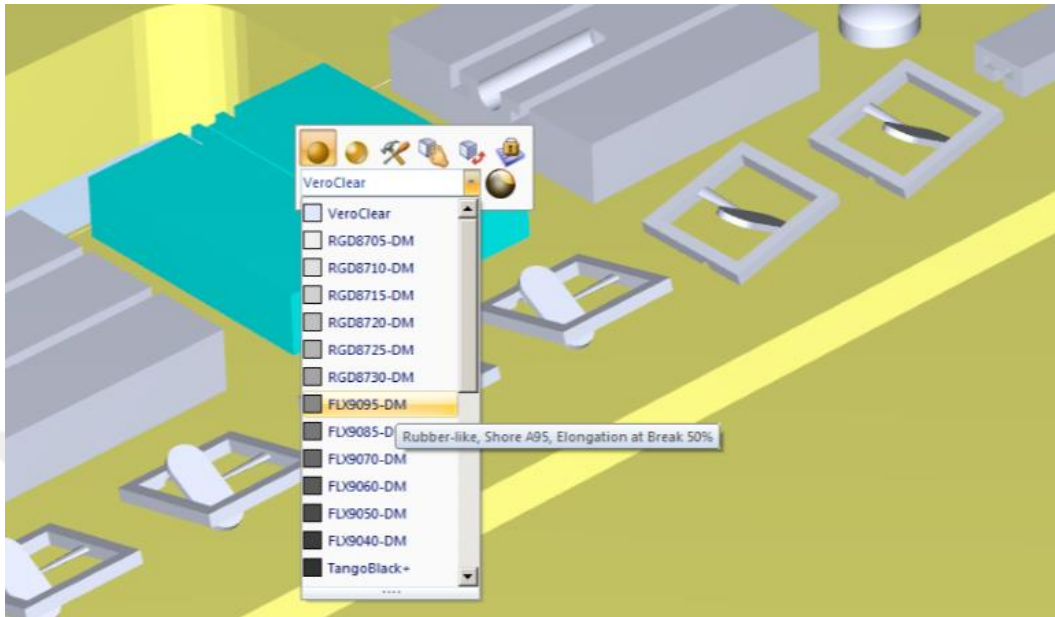


Figure A.5: Setting Position.



The printer allows two materials loaded into the nozzles at one time. From the software, the desired material or different concentrations of the mixture of these two materials (shown in Figure A.6) can be assigned to the whole model, or a piece of an assembled model.



**Figure A.6:** Selection of Materials.

Once all settings are assigned the user clicks on the “build tray” command then the printer starts depositing material. The printing process can be paused and continued from certain layers. Once the printing is finished, the structure is removed from the tray using a spatula and the tray needs to be cleaned with alcohol for the next printing.

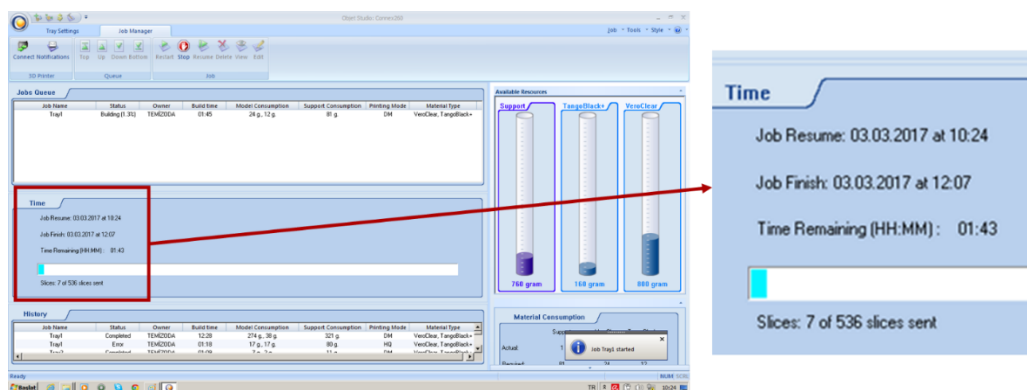


**Figure A.7:** Starting the Printing Process.

### **A.3. Finishing**

The structure which is covered in support material after the print must be cleaned properly. If the design is not extremely small or fragile, the support material can be removed with hand using brushes / alcohol and cotton.

If the structure's size is in micrometer levels and therefore fragile, it can be kept in a costic solution in a glass container for 1-2 days. Costic solution is prepared using NaOH and distilled water. The concentration of the costic solution can vary between %35-%40.

After the costic process, the structure is removed from the solution using gloves and washed carefully with water. Once the support material is eliminated, custom finishing processes can be used depending on the use of the print.

Costic solution with higher concentrations could damage the models that are not printed with high quality option. For these models water jet devices could also be employed.

## CURRICULUM VITAE



**Name Surname** : Janset Savaş  
**Place and Date of Birth** : İstanbul – 04.01.1992  
**E-Mail** : janset.savas@bilgi.edu.tr

### EDUCATION

- **B.Sc.** : 2015, İstanbul Bilgi Üniversitesi, Mühendislik Fakültesi, Elektrik Elektronik Mühendisliği

### PUBLICATIONS:

- **Janset Savaş** ; Ahmet Çalışkan ; Fehmi Çivitci ; Yiğit Dağhan Gökdel ; Onur Ferhanoğlu; “**Towards 3D Printed Confocal Endoscopy**” Proc. SPIE 9948, Novel Optical Systems Design and Optimization XIX, 99480D (September 28, 2016); doi:10.1117/12.2236641.  
<<http://proceedings.spiedigitallibrary.org/proceeding.aspx?articleid=2565178>>
- F. Sansal, **J.Savas**, Y.D.Gokdel, “**Comparison of 3D Printed and Regular Lens Performances on Laser Scanning Confocal Microscope**”, BMO München 2015, Munich, Germany
- A. Denker, **J. Savas**, A.U. Dilek, B, Sarioglu, Y.D. Gokdel, “**RoboSantral: An Autonomous Mobile Guide Robot**”, IEEE ICIT 2015, 17-19 March 2015, Sevilla, Spain.  
<<http://ieeexplore.ieee.org/abstract/document/7125141/>>